Criteria for Directly Detecting Topological Fermi Arcs in Weyl Semimetals

Ilya Belopolski, Su-Yang Xu, Daniel S. Sanchez, Guoqing Chang, Cheng Guo, Madhab Neupane, Hao Zheng, Chi-Cheng Lee, Shin-Ming Huang, Guang Bian, Nasser Alidoust, Tay-Rong Chang, BaoKai Wang, Xiao Zhang, Arun Bansil, Horng-Tay Jeng, Hsin Lin, Shuang Jia, and M. Zahid Hasan

Criteria for directly detecting topological Fermi arcs in Weyl semimetals

Ilya Belopolski*,[1, †] Su-Yang Xu*,[1] Daniel S. Sanchez*,[1] Guoqing Chang,[2, 3] Cheng Guo,[4] Madhab Neupane,[5] Hao Zheng,[1] Chi-Cheng Lee,[2, 3] Shin-Ming Huang,[2, 3] Guang Bian,[1] Nasser Alidoust,[1] Tay-Rong Chang,[1, 6] BaoKai Wang,[2, 3, 7] Xiao Zhang,[4] Arun Bansil,[7] Horng-Tay Jeng,[6, 8] Hsin Lin,[2, 3] Shuang Jia,[4] and M. Zahid Hasan[1, ‡]

[1]*Laboratory for Topological Quantum Matter and Spectroscopy (B7),*
Department of Physics, Princeton University, Princeton, New Jersey 08544, USA
[2]*Centre for Advanced 2D Materials and Graphene Research Centre,*
National University of Singapore, 6 Science Drive 2, Singapore 117546
[3]*Department of Physics, National University of Singapore, 2 Science Drive 3, Singapore 117542*
[4]*International Center for Quantum Materials, Peking University, Beijing 100871, China*
[5]*Condensed Matter and Magnet Science Group, Los Alamos National Laboratory, Los Alamos, NM 87545, USA*
[6]*Department of Physics, National Tsing Hua University, Hsinchu 30013, Taiwan*
[7]*Department of Physics, Northeastern University, Boston, Massachusetts 02115, USA*
[8]*Institute of Physics, Academia Sinica, Taipei 11529, Taiwan*
(Dated: January 14, 2016)

The recent discovery of the first Weyl semimetal in TaAs provides the first observation of a Weyl fermion in nature and demonstrates a novel type of anomalous surface state, the Fermi arc. Like topological insulators, the bulk topological invariants of a Weyl semimetal are uniquely fixed by the surface states of a bulk sample. Here, we present a set of distinct conditions, accessible by angle-resolved photoemission spectroscopy (ARPES), each of which demonstrates topological Fermi arcs in a surface state band structure, with minimal reliance on calculation. We apply these results to TaAs and NbP. For the first time, we rigorously demonstrate a non-zero Chern number in TaAs by counting chiral edge modes on a closed loop. We further show that it is unreasonable to directly observe Fermi arcs in NbP by ARPES within available experimental resolution and spectral linewidth. Our results are general and apply to any new material to demonstrate a Weyl semimetal.

A Weyl semimetal is a crystal which hosts Weyl fermions as emergent quasiparticles [1–10]. Although Weyl fermions are well-studied in quantum field theory, they have not been observed as a fundamental particle in nature. The recent experimental observation of Weyl fermions as electron quasiparticles in TaAs offers a beautiful example of emergence in science [11–21]. Weyl semimetals also give rise to a topological classification closely related to the Chern number of the integer quantum Hall effect [8–10, 22]. In the bulk band structure of a three-dimensional sample, Weyl fermions correspond to points of accidental degeneracy, Weyl points, between two bands [6, 7]. The Chern number on a two-dimensional slice of the Brillouin zone passing in between Weyl points can be non-zero, as illustrated in Fig. 1(a) [8–10]. Exactly as in the quantum Hall effect, the Chern number in a Weyl semimetal protects topological boundary modes. However, the Chern number changes when the slice is swept through a Weyl point, so the chiral edge modes associated with each slice terminate in momentum space at the locations of Weyl points, giving rise to Fermi arc surface states. This bulk-boundary correspondence makes it possible to demonstrate that a material is a Weyl semimetal by measuring Fermi arc surface states alone. As a result, to show novel Weyl semimetals, it is crucial to understand the possible signatures of Fermi
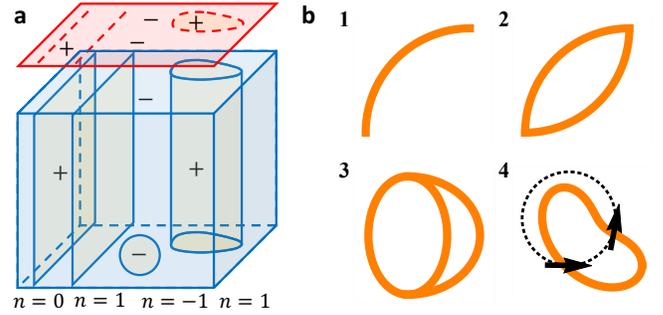

FIG. 1: **Four criteria for Fermi arcs.** (a) A bulk (blue) and surface (red) Brillouin zone with four Weyl points ($\pm$) and various 2D manifolds with Chern number n. Sweeping a plane through a Weyl point changes n. Also, any closed loop on the surface hosts chiral edge modes protected by the enclosed bulk chiral charge. For instance, a closed loop enclosing a + Weyl point will host one right-moving chiral edge mode [8–10]. (b) The criteria: (1) A disjoint contour. (2) A closed contour with a kink. (3) No kinks within experimental resolution, but an odd set of closed contours. (4) An even number of contours without kinks, but net non-zero chiral edge modes.

arcs in a surface state band structure.

Here, we present four distinct signatures of Fermi arcs, all in principle experimentally accessible in an ARPES measurement of a surface state band structure. Each signature alone, observed in any set of surface state bands, is sufficient to show that a material is a Weyl semimetal. Then, we apply these criteria to TaAs and NbP. We find

---

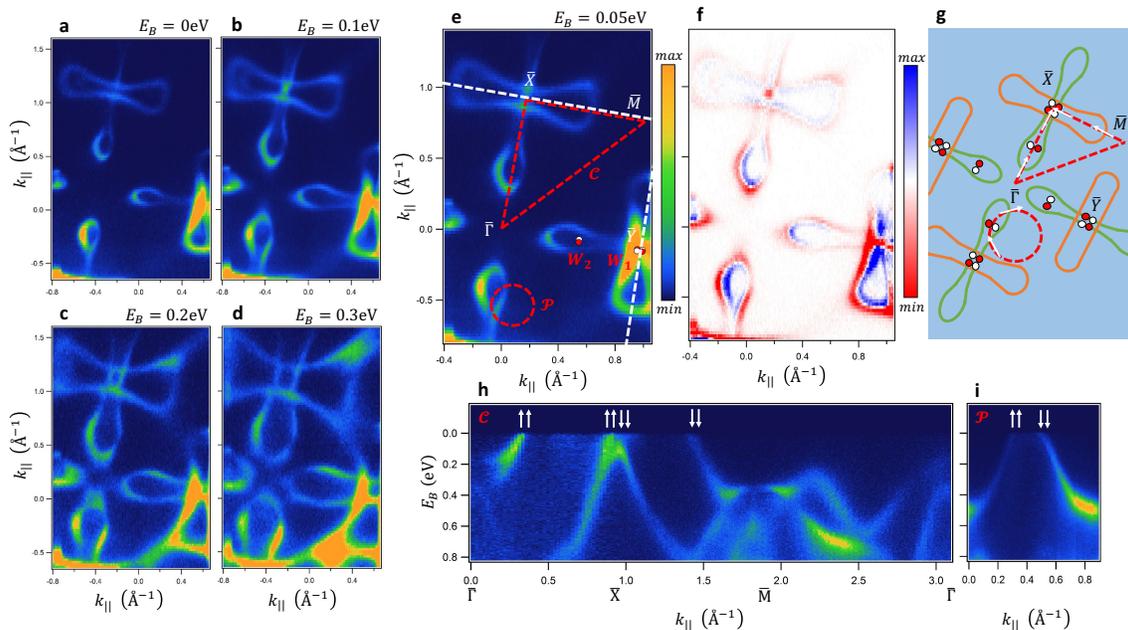*These authors contributed equally to this work.

FIG. 2: **Surface states of NbP by ARPES.** (a)-(d) Constant energy cut by vacuum ultraviolet APRES, at incident photon energy $h\nu = 30$eV, on the (001) surface of NbP. (e) Same as (a)-(d), at $E_B = 0.05$ eV, with Weyl points marked and the two paths $\mathcal{C}$ and $\mathcal{P}$ on which we measure Chern numbers. (f) The difference of ARPES spectra at $E_B = 0.05$ eV and $E_B = 0.1$ eV, illustrating the direction of the Fermi velocity all around the lollipop and peanut pockets. The blue contour is always inside the red contour, indicating that the sign of the Fermi velocity is the same going around each contour. This result excludes the possibility that the lollipop actually consists of Fermi arcs attached to the W_2. (g) Cartoon summarizing the band structure. (h) Band structure along $\mathcal{C}$, with chiralities of edge modes marked by the arrows. We associate one arrow to each spinful crossing, even where we cannot observe spin splitting due to the weak SOC of NbP. There are the same number of arrows going up as down, so the Chern number is zero. (i) Same as (h) but along $\mathcal{P}$. Again, the Chern number is zero.

that we can rigorously demonstrate a Weyl semimetal in TaAs by directly measuring a non-zero Chern number in ARPES. For NbP, we find that it is unreasonable to directly observe Fermi arcs within experimental resolution because the spin-orbit coupling is too weak.

Any surface state band structure which satisfies any one of the following four conditions contains topological Fermi arcs and is necessarily a Weyl semimetal:

1. *Disjoint arc*: Any surface state constant-energy contour with an open curve is a Fermi arc and demonstrates a Weyl semimetal.

2. *Kink off a rotation axis*: A Weyl point is characterized by chiral charge n, equal to the Chern number on a small spherical manifold enclosing the Weyl point in the bulk Brillouin zone, illustrated by the small sphere in Fig. 1(a) [8–10]. For a Weyl point of chiral charge $|n| > 1$ or if multiple Weyl points project onto the same point of the surface Brillouin zone, there may not be a disjoint constant-energy contour because multiple arcs will emanate from the same Weyl point projection. However, the arcs will generically attach to the Weyl point at different slopes, giving rise to a kink in the constant-energy contour. Moreover, such a kink can only arise from

the attachment of two Fermi arcs. A kink on the projection of a rotation axis may arise in a topological Dirac semimetal [23]. Off a rotation axis, such a kink guarantees a Weyl semimetal.

3. *Odd number of curves*: For projected chiral charge $|n| > 1$, the constant-energy contours may consist entirely of closed curves and the kink may be below experimental resolution, so the constant-energy contour appears everywhere smooth. However, if $|n|$ is odd, the constant-energy contour will consist of an odd number of curves, so at least one curve must be a Fermi arc.

4. *Non-zero Chern number*: Consider any closed loop in the surface Brillouin zone where the bulk band structure is everywhere gapped and, at some energy, add up the signs of the Fermi velocities of all surface states along this curve, with $+1$ for right movers and -1 for left movers. The sum is the projected chiral charge enclosed in the curve, corresponding to a Chern number on a bulk [8–10]. A non-zero sum on at least one loop demonstrates a Weyl semimetal, provided the loop is chosen to be contractible on the torus formed by the surface Brillouin zone.
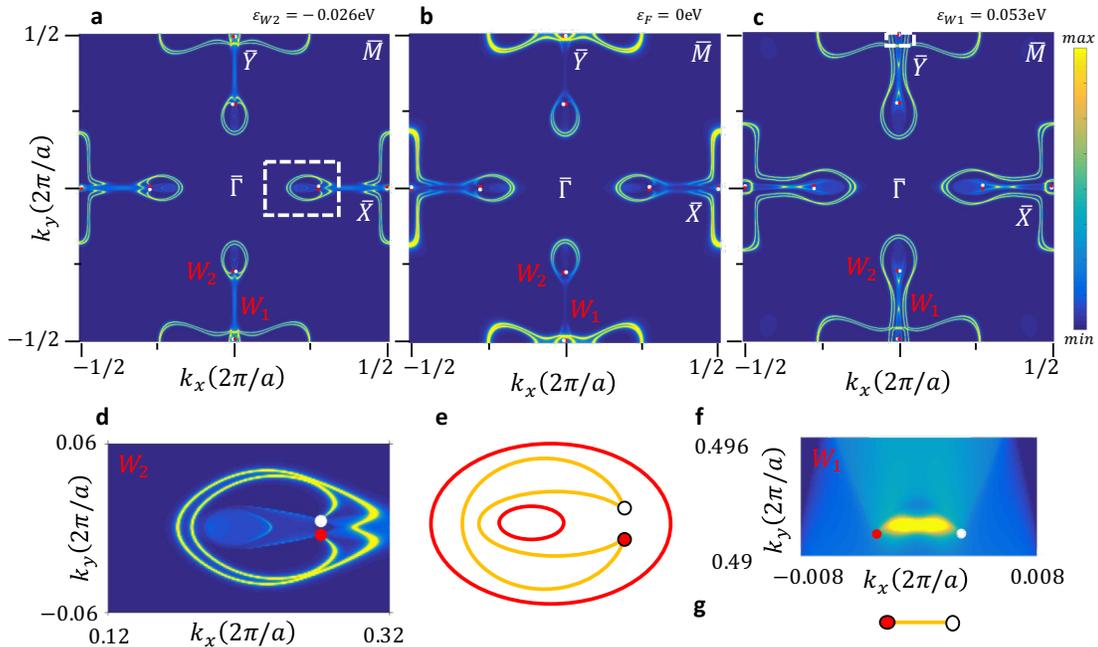
FIG. 3: **Numerical calculation of Fermi arcs in NbP.** First-principles band structure calculation of the (001) surface states of NbP at (a) the energy of the W_2, above the Fermi level, (b) the Fermi level and (c) the energy of the W_1, below the Fermi level. In (a) we see (1) a small set of surface states near the W_2 and (2) larger surface states near $\bar{X}$ and $\bar{Y}$. Near the energy of (b) there is a Lifshitz transition between the surface states at (1) and (2), giving rise to lollipop and peanut-shaped pockets. At (c) we see that the lollipop and peanut pockets enlarge, so they are hole-like. We also observe short Fermi arcs connecting the W_1. The numerical calculation shows excellent overall agreement with our ARPES spectra, suggesting that NbP is a Weyl semimetal. (d) Zoom-in of the surface states around the W_2, indicated by the white box in (a). We find two Fermi arcs and two trivial closed contours, illustrated in (e). (f) Zoom-in of the surface states around W_1, indicated by the white box at the top of (c). We find one Fermi arc, illustrated in (g).

Note that while (1), (2) and (3) describe properties of a constant-energy slice of the Fermi surface, the counting argument (4) requires a measurement of the dispersion. We note also that criterion (4) allows us to determine all bulk topological invariants and Weyl points of a material by studying only its surface states.

In the rest of this Letter, we apply these criteria to TaAs and NbP. We find that criterion (4) shows a Weyl semimetal in TaAs, but that all criteria fail for NbP because the spin-orbit coupling is too weak and the Fermi level is too low. We also present a calculation of NbP and show that it may be possible to demonstrate a Fermi arc in NbP by ARPES by observing a kink, criterion (2), but only if the Fermi level can be raised > 20 meV. Lastly, we point out that the counting argument (4) as recently applied to TaAs [15, 20] and NbP [24] is invalid because certain Weyl points are too close together.

Single crystal TaAs and NbP samples were grown by chemical vapor transport methods. Angle-resolved photoemission spectroscopy (ARPES) measurements were performed using a Scienta R4000 at Beamline 5-4 of the Stanford Synchrotron Radiation Lightsource, SLAC and Beamline 4 of the Advanced Light Source, LBNL in CA,

USA. The angular resolution was better than $0.2°$ and the energy resolution better than 20meV. Samples were cleaved *in situ* and measured under vacuum better than 10^{-10} Torr at temperatures < 30K. First principles electronic structure calculations of NbP were carried out with the OpenMX code [27], based on the generalized gradient approximation (GGA) [28]. Spin-orbit coupling was incorporated through j-dependent pseudo-potentials. For each Nb atom three, three, three and one optimized radial functions were allocated for the s, p, d, and f orbitals ($s3p3d3f1$), respectively. For each P atom, $s3p3d2f1$ were adopted. A k-point mesh of $17 \times 17 \times 5$ for the conventional unit cell was used and experimental lattice parameters were adopted in the calculations [29–31]. We use Nb s and d orbitals and P p orbitals to construct Wannier functions without performing the procedure for maximizing localization [32, 33]. We calculated the surface spectral weight of a semi-infinite (001) slab using an iterative Green's function method based on the Wannier function basis set.

We show that the surface state band structure of NbP as measured by ARPES does not satisfy any of the Fermi arc criteria. We note that vacuum ultraviolet ARPES is
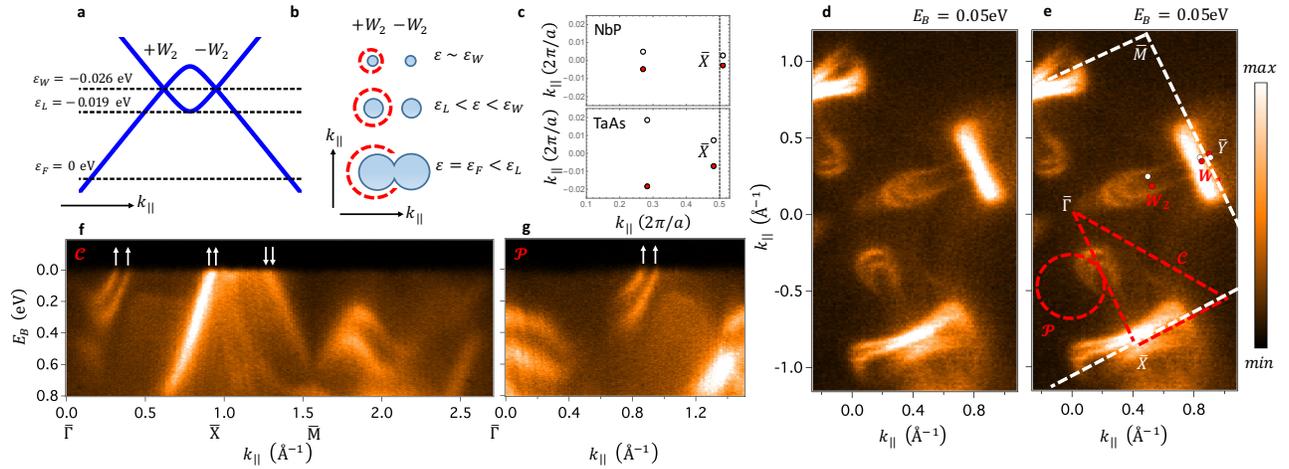
FIG. 4: **Comparison of NbP and TaAs.** (a) Energies of the W_2, their Lifshitz transition and the Fermi level from the numerical calculation. One consequence of the small spin-splitting is that the Lifshitz transition between the W_2 is only ~ 0.007 eV below the energy of the W_2 and ~ 0.019 eV above the Fermi level. (b) Because $\varepsilon_F < \varepsilon_L$, it makes no sense to calculate the Chern number on $\mathcal{C}$ and $\mathcal{P}$, because the system on that cut is not an insulator, see the interrupted dotted red line in the last row of (b). (c) Plot of the positions of the Weyl point projections in NbP and TaAs arising from one Dirac line (see §1, SI). We see that the separation of the Weyl points is ~ 4 times larger in TaAs due to the large SOC. (d) Fermi surface by vacuum ultraviolet APRES, at incident photon energy $h\nu = 90$eV, on the (001) surface of TaAs. (e) Same as (d), but with Weyl points marked and two paths $\mathcal{C}$ and $\mathcal{P}$. (f) Band structure along $\mathcal{C}$, with chiralities of edge modes marked by the arrows. The net Chern number appears to be $+2$, inconsistent with the calculation. This can be explained by considering the small separation between the W_1. (g) Same as (f) but along $\mathcal{P}$. The path encloses only the well-spaced Weyl points and we find a Chern number $+2$, consistent with the calculation.

sensitive to the surface states of NbP, see Supplementary Information (SI). The surface states consist of lollipop and peanut-shaped pockets and we find that both are hole-like, see Figs. 2(a)-(d). *Criterion (1).* Both the lollipop and peanut pockets are closed, so we observe no single disconnected arc. *Criterion (2).* We see no evidence of a kink in the constant-energy contours, so we do not observe a pair of arcs connecting to the same W_2 in a discontinuous way. *Criterion (3).* We observe an even number of contours everywhere, so no arc. *Criterion (4).* We can study the Fermi velocity using a difference map of two ARPES spectra, at $E_B = 0.05$ eV and $E_B = 0.1$ eV, shown in Fig. 2(f). We see that the Fermi velocities have the same sign all the way around both the lollipop and the peanut pockets. If the lollipop consisted of Fermi arcs, one arc should evolve in a hole-like way, while the other arc should evolve in an electron-like way, so the different regions of the lollipop pocket should have opposite Fermi velocities in this sense. Because all points on both pockets have the same Fermi velocity, within the resolution of our ARPES measurements these pockets are trivial, hole-like surface states, and we observe no topological Fermi arcs. We can also consider a closed path through the surface Brillouin zone and count chiralities of edge modes along the path, illustrated in Figs. 2(e,g). We check a triangular path, $\mathcal{C}$, along $\bar{\Gamma}-\bar{X}-\bar{M}-\bar{\Gamma}$, which encloses net chiral charge $+1$, Fig. 2(h), and a small circular path, $\mathcal{P}$, which encloses net chiral charge -2, Fig.

2(i). For each path, we label each spinless crossing with an up or down arrow to indicate the sign of the Fermi velocity. We find that going around either $\mathcal{C}$ and $\mathcal{P}$ we have net zero chirality, showing zero Chern number on the associated bulk manifold. The surface states of NbP fail all criteria for Fermi arcs. We cannot show that NbP is a Weyl semimetal using only the surface state band structure from ARPES.

Next, we compare our experimental results to numerical calculations on NbP and show that it is challenging to observe Fermi arcs in our spectra because of the low spin-orbit coupling. We present a calculation of the (001) surface states in NbP for the P termination, at the binding energy of W_2, $\varepsilon_{W2} = -0.026$ eV, at the Fermi level and at the binding energy of W_1, $\varepsilon_{W1} = 0.053$ eV, see Figs. 3(a)-(c). We also plot the Weyl point projections, obtained from a bulk band structure calculation [34]. We observe surface states (1) near the mid-point of the $\bar{\Gamma}-\bar{X}$ and $\bar{\Gamma}-\bar{Y}$ lines and (2) near $\bar{Y}$ and $\bar{X}$. The surface states (1) form two Fermi arcs and two closed contours at ε_{W2}, see Fig. 3(d),(e). These states undergo a Lifshitz transition near ε_F with the surface states (2), forming a large hole-like pocket below the Fermi level. The surface states (2) also form a large hole-like pocket. They contain within them, near the $\bar{X}$ and $\bar{Y}$ points, a short Fermi arc connecting each pair of W_1, see Fig. 3(f),(g). We note the excellent agreement with our ARPES spectra, where we also see lollipop and peanut contours which

evolve into trivial, closed, hole-like pockets below ε_F. At the same time, we find in our calculation that the separation of Weyl points and the spin-splitting in the surface states is small. This result is consistent with our ARPES spectra, which do not show spin-splitting in the surface states near the Fermi level.

The small spin-splitting observed in our numerical calculations underlines the difficulty in observing topological Fermi arc surface states in NbP. The separation of the Weyl points is $< 0.01\text{Å}^{-1}$ for the W_1 and $< 0.02\text{Å}^{-1}$ for the W_2, both well below the typical linewidth of our ARPES spectra, $\sim 0.05\text{Å}^{-1}$. For this reason, we cannot resolve the momentum space region between the W_1 or the W_2 to determine if there is an arc. We emphasize that we cannot surmount this difficulty by considering Fermi level crossings on $\mathcal{P}$ or $\mathcal{C}$, as shown in Fig. 2(e). It is obvious that if we cannot resolve the two Weyl points in a Fermi surface mapping, then we also cannot resolve a Fermi arc connecting them in a cut passing through the Weyl points. In this way, on $\mathcal{P}$ we cannot verify the arc connecting the W_1 and on $\mathcal{P}$ and $\mathcal{C}$ we cannot verify the empty region between the W_2. As an additional complication, it is difficult to use $\mathcal{P}$ or $\mathcal{C}$ because the Fermi level is below the Lifshitz transition for the W_2 in NbP, see Fig. 4a. This invalidates use of criterion (4) because for $\varepsilon_F < \varepsilon_L$, there is no accessible binding energy where the bulk band structure is gapped along an entire loop passing in between a pair of W_2, illustrated in Fig. 4b by the broken dotted red line for $\varepsilon = \varepsilon_F$. However, if we could access $\varepsilon > \varepsilon_L$, then it may be possible to use criterion (2) to demonstrate a Fermi arc in NbP without resolving the W_2 and counting chiralities. In particular, while the Fermi arc may appear to form a closed contour due to the small separation of W_2, it could have a kink at the location of the W_2. Unlike criterion (4), applying criterion (2) to (001) NbP would not depend on resolving the W_2 or the spin-splitting of the surface states. Improvements in the quality of NbP crystals or the cleaved surface could also allow the Fermi arcs to be resolved by reducing the spectral linewidth. Lastly, we point out that our results invalidate recent claims that $\mathcal{C}$ [24] or any direct measurement of Fermi arcs [25, 26] can be used to demonstrate a Weyl semimetal in NbP, due to the large linewidth of available ARPES spectra.

We apply criterion (4) to demonstrate Fermi arcs in TaAs. The larger spin-splitting in TaAs increases the separation of Weyl points as compared to NbP, see Fig. 4c. However, we emphasize that only the W_2 are well within experimental resolution. The separation of the W_1 in TaAs is comparable to the separation of the W_2 in NbP, which as noted above, cannot be resolved. In contrast to NbP, the (001) surface states of TaAs near $\bar{\Gamma}$ consist of crescent pockets with clear spin-splitting, see Fig. 4(d). We also observe bowtie surface states near $\bar{X}$ and $\bar{Y}$. We apply criterion (4) to search for Fermi arcs

in TaAs on paths $\mathcal{C}$ and $\mathcal{P}$, shown in Fig. 4(e). We mark the Fermi velocity of each crossing with an arrow, but now with one arrow per spinful crossing. Along $\mathcal{C}$, see Fig. 4(f), we see two well-resolved crossings not far from $\bar{\Gamma}$. However, the spinful crossings from the bowtie pocket are difficult to resolve. Based on the constant-energy contour, Fig. 4(d), we may interpret the bowtie pocket as consisting of two slightly-separated spinful contours, so we associate two arrows with each of the remaining two crossings along $\mathcal{C}$. We find that the enclosed Chern number is $+2$, while it is $+3$ according to a numerical calculation of the band structure [34]. Again, this inconsistency results from the small separation of the W_1. As a result, we cannot resolve the additional crossing from the Fermi arc connecting the W_1 near $\bar{X}$, which would give a Chern number of $+3$. We can avoid the bowtie pocket by using $\mathcal{P}$, see Fig. 4g. Here, we see only the two well-separated states near $\bar{\Gamma}$. We find two edge modes of the same chirality, unambiguously showing a Chern number $+2$ on the associated bulk manifold, satisfying criterion (4) for a Weyl semimetal. In this way, we demonstrate that TaAs is a Weyl semimetal by studying only the surface states as measured by ARPES. We note that our results invalidate earlier measurements on $\mathcal{C}$ used to demonstrate a Weyl semimetal in TaAs [15, 20]. Here, we have shown that the small separation between the W_1 in TaAs makes it impossible to calculate the Chern number on $\mathcal{C}$. In the same way, our results on NbP invalidate recent works claiming a Weyl semimetal in NbP using $\mathcal{C}$ [24] or by directly observing Fermi arcs [25, 26]. We emphasize that to show a Weyl semimetal it is not enough to present an overall agreement between ARPES and numerics. In the case of TaAs and NbP, there are many trivial surface states, so an overall agreement is not entirely relevant for the topological invariants or the Weyl semimetal state. In addition, an overall agreement is precarious in cases where the system is near a critical point or where there may be several closely-related crystal structures. Rather, to show a Weyl semimetal, it is sufficient to pinpoint a topological Fermi arc in an ARPES spectrum of surface states. Here, we have presented a set of general and distinct criteria, applicable to any material, any one of which pinpoints a topological Fermi arc. By presenting criteria for Fermi arcs, we provide a useful reference for demonstrating novel Weyl semimetals.

---

† Electronic address: ilyab@princeton.edu

‡ Electronic address: mzhasan@princeton.edu

[1] H. Weyl. Z. Phys. **56**, 330 (1929).

[2] C. Herring. Phys. Rev. **52**, 365 (1937).

[3] A. A. Abrikosov & S. D. Beneslavskii. J. Low Temperature Physics **5**, 141 (1971).

[4] H. B. Nielsen & M. Ninomiya. Phys. Lett. B **130**, 389 (1983).

[5] G. E. Volovik, *The Universe in a Helium Droplet* (Clarendon Press, Oxford, 2003).

[6] S. Murakami. New Journal of Physics **9**, 356 (2007).

[7] A. A. Burkov & L. Balents. Phys. Rev. Lett. **107**, 127205 (2011).

[8] X. Wan, A. M. Turner, A. Vishwanath & S. Y. Savrasov. Phys. Rev. B **83**, 205101 (2011).

[9] A. Turner & A. Vishwanath. arXiv:1301.0330.

[10] P. Hosur & X. Qi. Comp. Rend. Phy. **14**, 857 (2013).

[11] S.-M. Huang, S.-Y. Xu, I. Belopolski, C.-C. Lee, G. Chang, B. K. Wang, N. Alidoust, G. Bian, M. Neupane, C. Zhang, S. Jia, A. Bansil, H. Lin & M. Z. Hasan. Nat. Commun. **6**, 7373 (2015).

[12] H. Weng, C. Fang, Z. Fang, B. A. Bernevig & X. Dai. Phys. Rev. X **5**, 011029 (2015).

[13] S.-Y. Xu, I. Belopolski, N. Alidoust, M. Neupane, G. Bian, C. Zhang, R. Sankar, G. Chang, Z. Yuan, C.-C. Lee, S.-M. Huang, H. Zheng, J. Ma, D. S. Sanchez, B. K. Wang, A. Bansil, F. C. Chou, P. P. Shibayev, H. Lin, S. Jia & M. Z. Hasan. Science **349**, 613 (2015).

[14] L. Lu, Z. Wang, D. Ye, L. Ran, L. Fu, J. D. Joannopoulos & M. Soljačić. Science **349**, 622 (2015).

[15] B. Q. Lv, H. M. Weng, B. B. Fu, X. P. Wang, H. Miao, J. Ma, P. Richard, X. C. Huang, L. X. Zhao, G. F. Chen, Z. Fang, X. Dai, T. Qian & H. Ding. Phys. Rev. X **5**, 031013 (2015).

[16] B. Q. Lv, N. Xu, H. M. Weng, J. Z. Ma, P. Richard, X. C. Huang, L. X. Zhao, G. F. Chen, C. E. Matt, F. Bisti, V. N. Strocov, J. Mesot, Z. Fang, X. Dai, T. Qian, M. Shi & H. Ding. Nat. Phys. **11**, 724 (2015).

[17] S.-Y. Xu, N. Alidoust, I. Belopolski, Z. Yuan, G. Bian, T.-R. Chang, H. Zheng, V. N. Strocov, D. S. Sanchez, G. Chang, C. Zhang, D. Mou, Y. Wu, L. Huang, C.-C. Lee, S.-M. Huang, B. K. Wang, A. Bansil, H.-T. Jeng, T. Neupert, A. Kaminski, H. Lin, S. Jia & M. Z. Hasan. Nat. Phys. **11**, 748 (2015).

[18] S.-Y. Xu, I. Belopolski, D. S. Sanchez, C. Zhang, G. Chang, C. Guo, G. Bian, Z. Yuan, H. Lu, T.-R. Chang, P. P. Shibayev, M. L. Prokopovych, N. Alidoust, H. Zheng, C.-C. Lee, S.-M. Huang, R. Sankar, F. C. Chou, C.-H. Hsu, H.-T. Jeng, A. Bansil, T. Neupert, V. N. Strocov, H. Lin, S. Jia & M. Z. Hasan. Sci. Adv. **1**, 10 (2015).

[19] N. Xu, H. M. Weng, B. Q. Lv, C. Matt, J. Park, F. Bisti, V. N. Strocov, D. Gawryluk, E. Pomjakushina, K. Conder, N. C. Plumb, M. Radovic, G. Autès, O. V. Yazyev, Z. Fang, X. Dai, G. Aeppli, T. Qian, J. Mesot, H. Ding & M. Shi. arXiv:1507.03983.

[20] L. X. Yang, Z. K. Liu, Y. Sun, H. Peng, H. F. Yang, T. Zhang, B. Zhou, Y. Zhang, Y. F. Guo, M. Rahn, D. Prabhakaran, Z. Hussain, S.-K. Mo, C. Felser, B. Yan & Y. L. Chen. Nat. Phys. **11**, 728 (2015).

[21] H. Zheng, S.-Y. Xu, G. Bian, C. Guo, G. Chang, D. S. Sanchez, I. Belopolski, C.-C. Lee, S.-M. Huang, X. Zhang, R. Sankar, N. Alidoust, T.-R. Chang, F. Wu, T. Neupert, F. C. Chou, H.-T. Jeng, N. Yao, A. Bansil, S. Jia, H. Lin & M. Z. Hasan. ACS Nano. DOI:10.1021/acsnano.5b06807 (2015).

[22] A. Bernevig & T. Hughes, *Topological Insulators and Topological Superconductors* (Princeton University Press, Princeton, 2013).

[23] S.-Y. Xu, C. Liu, S. K. Kushwaha, R. Sankar, J. W. Krizan, I. Belopolski, M. Neupane, G. Bian, N. Alidoust, T.-R. Chang, H.-T. Jeng, C.-Y. Huang, W.-F. Tsai, H. Lin, P. P. Shibayev, F. C. Chou, R. J. Cava & M. Z. Hasan. Science **347**, 294 (2015).

[24] D.-F. Xu, Y.-P. Du, Z. Wang, Y.-P. Li, X.-H. Niu, Q. Yao, P. Dudin, Z.-A. Xu, X.-G. Wan & D.-L. Feng. Chin. Phys. Lett. **32**, 10 (2015).

[25] S. Souma, Z. Wang, H. Kotaka, T. Sato, K. Nakayama, Y. Tanaka, H. Kimizuka, T. Takahashi, K. Yamauchi, T. Oguchi, K. Segawa & Y. Ando. arXiv:1510.01503.

[26] Z. K. Liu, L. X. Yang, Y. Sun, T. Zhang, H. Peng, H. F. Yang, C. Chen, Y. Zhang, Y. F. Guo, D. Prabhakaran, M. Schmidt, Z. Hussain, S.-K. Mo, C. Felser, B. Yan & Y. L. Chen. Nat. Mat. (2015).

[27] T. Ozaki. Phys. Rev. B **67**, 155108 (2003).

[28] J. P. Perdew, K. Burke & M. Ernzerhof. Phys. Rev. Lett. **77**, 3865 (1996).

[29] S. Rundqvist. Nature **211**, 847 (1966).

[30] J. O. Willerström. J. Less Common Metals **99**, 273 (1984).

[31] J. Xu, M. Greenblatt, T. Emge & P. Höhn. Inorgan. Chem. **35**, 845 (1996).

[32] N. Marzari & D. Vanderbilt. Phys. Rev. B **56**, 12847 (1997).

[33] A. A. Mostofi, J. R. Yates, Y.-S. Lee, I. Souza, D. Vanderbilt & N. Marzari. Comp. Phys. Commun. **178**, 685 (2008).

[34] C.-C. Lee, S.-Y. Xu, S.-M. Huang, D. S. Sanchez, I. Belopolski, G. Chang, G. Bian, N. Alidoust, H. Zheng, M. Neupane, B. K. Wang, A. Bansil, M. Z. Hasan & H. Lin. Phys. Rev. B **92**, 235104 (2015).